International Journal of Nanomedicine

Dovepress
open access to scientific and medical research

Open Access Full Text Article

ORIGINAL RESEARCH

Enhancing the Inhibition of Corneal Neovascularization Efficacy by Self-Assembled into Supramolecular Hydrogel of Anti-Angiogenic Peptide

Guojuan Pu[1,2], Zhen Liang[1,2], Jieran Shi[2], Yuan Tao[1,2], Ping Lu[1,2], Huiling Qing[1,2], Junjie Zhang[1,2]

[1]Henan Eye Hospital, Henan Eye Institute, Henan Provincial People's Hospital, Zhengzhou, 450003, People's Republic of China; [2]People's Hospital of Zhengzhou University, Zhengzhou, 450003, People's Republic of China

Correspondence: Junjie Zhang, Henan Eye Hospital, Henan Eye Institute, Henan Provincial People's Hospital, and People's Hospital of Zhengzhou University, Number 7 Weiwu Road, Zhengzhou, 450003, People's Republic of China, Email zhangjunjie@zzu.edu.cn

Background: Corneal neovascularization (CNV) is a common eye disease that leads to blindness. New treatment strategies are urgently needed due to the limitations of current treatment methods.

Methods: We report the synthesis of peptide Nap-FFEEPCAIWF (***Comp.3***) via chemical conjugation of Nap-FFEE (***Comp.2***) to antiangiogenic peptide PCAIWF ***(Comp.1)***. ***Comp.3*** self-assembled into a hydrogel (***gel of 3***) composed of nanofibers, which enhanced the antiangiogenic function of the epitope.

Results: We developed a novel peptide with an amphiphilic framework, ***Comp.3***, which could self-assemble into a supramolecular hydrogel with a well-ordered nanofiber structure. The nanofibers exhibited good biocompatibility with corneal epithelial cells, presenting a promising strategy to enhance the efficacy of free peptide–based drugs in the treatment of ocular vascular diseases, such as CNV and other angiogenesis-related diseases.

Conclusion: Nap-FFEEPCAIWF nanofibers provide an alternative approach to enhancing the therapeutic efficiency of free peptide–based drugs against ocular vascular diseases.

Keywords: antiangiogenic peptide, self-assembled, hydrogel, nanofiber, corneal neovascularization

Introduction

The healthy cornea is transparent, avascular, clear, and immune-privileged structure of the anterior eye.[1,2] The cornea maintains the state of avascularity by balancing antiangiogenetic and angiogenetic factors. Chemical burns, infectious keratitis, herpes eye, surgery, and inflammation can break down the balance of avascularity, leading to corneal neovascularization (CNV),[3–7] which can cause vision loss and severe visual impairment.[8] CNV remains challenging to cure clinically.[9] Pathological neovascularization is usually associated with hypoxic stimuli, oxidative stress, matrix metalloproteinases, overexpression of inflammatory factors, and vascular endothelial growth factor (VEGF).[10–13] Inhibiting the activity of VEGF and its receptors, which play vital roles in the angiogenic process, has been demonstrated to be an effective means of treating CNV.[14–17] In recent years, ranibizumab and bevacizumab have been utilized in CNV treatment to improve the vision of patients with abnormal ocular angiogenesis.[18,19] However, some patients present an insufficient response to such treatments or their symptoms worsen due to resistance or injury, and manufacturing difficulties, high costs, metabolic instability, and short half-lives further limit the use of bevacizumab and other antibody drugs.[20,21] Therefore, new therapeutic formulations capable of eliminating these disadvantages are urgently needed.[22]

Peptides are usually employed in mediated targeting strategies, demonstrating considerable potential to suppress the activity of angiogenic factors and good efficacy, safety, high selectively, and modifiable properties compared with

Received: 17 April 2024
Accepted: 10 July 2024
Published: 25 July 2024

Graphical Abstract

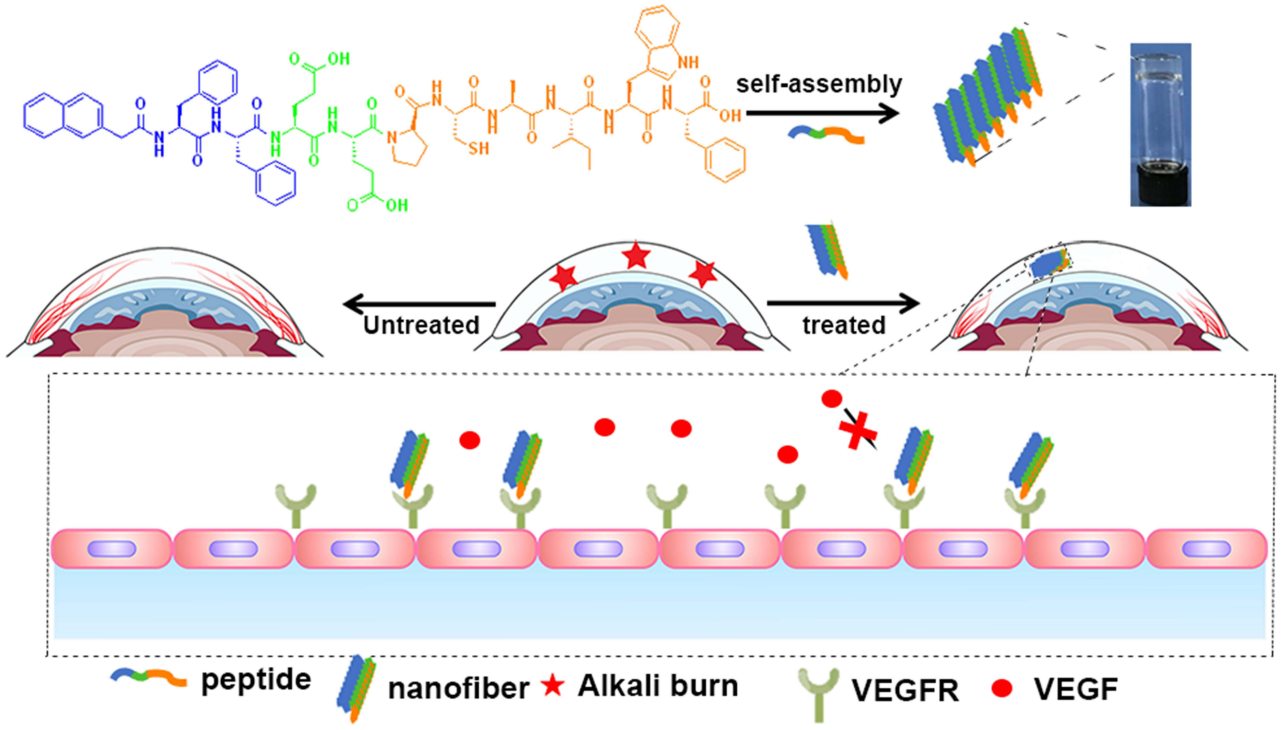

proteins[23–25]. In the past few years, researchers have designed several antagonist peptides using a rational approach.[26–31] Among them, the PCAIWF (***Comp.1***) peptide sequence has been proven to target the extracellular ligand–binding domain of all three VEGF receptors.[32] However, its short half-life, low solubility, and instability limit its administration routes. To solve these issues, we developed an antiangiogenic peptide–based nanostructure to improve the biological activity and antiangiogenic efficacy of ***Comp.1***.

Supramolecular self-assembly of peptides has demonstrated great potential in biomaterial fields such as tissue engineering, biopharmaceuticals, and various ocular disease therapies.[33–36] Supramolecular self-assembled peptides with an amphiphilic framework are composed of hydrophobic and hydrophilic peptide segments.[37–43] In this study, the peptide Nap-FFEE (***Comp.2***) was conjugated to bioactive peptide ***Comp.1*** via a chemical method to obtain Nap-FFEEPCAIWF (***Comp.3***), which self-assembled into a hydrogel (***gel of 3***) with a nanofiber (NF) structure. Intriguingly, the obtained NFs increased the water solubility of the peptide and emerged as a functional epitope. ***Comp.3*** enhanced the antiangiogenic capacity of the peptide, which was evaluated through in vitro angiogenesis experiments and cell tube formation assays. Moreover, the effect of the NFs was studied in the CNV mouse model induced by alkali burn. Further, the bioactive NFs demonstrated high efficiency and biocompatibility in vitro and in vivo.

Materials and Methods

Materials and Animals

Materials

2-Cl-trityl chloride resin was obtained from Nankai University Resin Co. Ltd. (Tianjin, China). Fmoc-based amino acids were obtained from GL Biochem (Shanghai, China). Commercially available reagents were employed without further purification, unless noted otherwise. Nanopure water was utilized for all experiments. All other chemicals were of reagent grade or better. N, N-Diisopropylethylamine was obtained from J&K Scientific Co. Ltd. (Beijing, China). Dexamethasone sodium phosphate eye drops (Dex) were purchased from Huaqing Pharmaceutical (Xinxiang, China).

The cell counting kit-8 (CCK-8) and BCA assay kit were obtained from Beyotime (Shanghai, China). VEGF-A (AF-293-NA) and VEGF-C (AF752) antibodies were purchased from the R&D Systems (USA). VEGF-A and VEGF-C ELISA kits were purchased from Elabscience Biotechnology (Wuhan, China).

Animals

Eighty 6–8 week–old male BALB/c mice, weighing 18–22 g, were purchased from Huaxing Experimental Animal Farm (Zhengzhou, China), New Zealand White rabbits, weighing 2.0–2.5 kg), obtained from the same place. All animals freely consumed standard feed and drinking water and were raised in a room maintained at 25.0°C with a 12 h:12 h light–dark cycle. All experimental animal procedures were approved by the Experimental Animal Ethics Committee of Henan Institute of Ophthalmology (HNEECA-2023-04) and complied with National Institutes of Health guidelines. All procedures in the study conformed to the ARVO statement.

Peptide Synthesis and Characterization of Self-Assembly

Peptide Synthesis

The peptides were synthesized by traditional solid-phase peptide synthesis (SPPS) using 2-chlorotrityl chloride resin, and the corresponding N-Fmoc protected each amino acid, with the side chains appropriately protected by different groups. The first amino acid was placed on the resin at the C-terminal, and the loading efficiency was approximately 1.2 mmol/g. The Fmoc group was deprotected from the amino acid by 20% piperidine in anhydrous N, N′-dimethylformamide (DMF). Then, the next Fmoc-protected amino acid was coupled to the free amino group using HBTU as the coupling reagent. The peptide chain was grown according to the Fmoc SPPS protocol. After the last coupling step, the residual reagent was removed by washing the resin with DMF 5 times (10 mL per gram of resin, for 1 min each), followed by washing the resin with DCM 5 times (5 mL per gram of resin, for 1 min each). The peptides were cleaved from the resin using 95% trifluoroacetic acid (TFA) with 2.5% TIS and 2.5% H_2O for 0.5 h, and excess TFA was removed. Diethyl ether (50 mL per gram of resin) was then added to the cleavage reagent, and the resulting precipitate was collected. The obtained crude peptides were further dried in vacuo and purified by high-performance liquid chromatography (HPLC). The final obtained pure peptides were characterized by high-resolution mass spectrometry (HR-MS).

Hydrogel Formation

Comp.3 (2.5 mg) was suspended in 0.5 mL of PBS, and the suspension was adjusted to pH 7.4 using Na_2CO_3, after which the suspension was through the heating-cooling process to form hydrogel.

Rheology

The oscillatory rheological properties of formed hydrogels were measured using a rheometer (MCR302, Anton Pa, Austria). Hydrogel (0.5 mL) was loaded onto the 25 mm cone plate for the experiment. The frequency sweep test of the hydrogel was performed in the range of 0.1–100 rad/s at a constant strain of 1%.

Transmission Electron Microscopy (TEM)

Samples of hydrogel were prepared. Next, 10 μL samples for TEM (Talos F200C, Thermo Fisher Scientific, USA) analysis by loading on a 400-mesh copper grid for 30s to adhere the peptide nanostructure to the substrate. The sample was then stained with saturated uranyl acetate solution and placed in a desiccator overnight before analysis.

UV Spectroscopy

The UV–Vis optical spectra of self-assemblies were measured using a UV–Vis spectrophotometer (UV-1800SPC, Macylab Instrument Inc, China). The path length of the cuvette was 1 cm, the detection range was set to 200–600 nm, and the spectral resolution was set to 1.0 nm.

Circular Dichroism (CD)

CD (Chirascan V100, Applied Photophysics Ltd., England) characterizations were performed using a 0.5 mm thick standard quartz cell at room temperature. The CD spectra were measured from 185 nm to 300 nm at a step size of 0.5 nm.

Cell Culture Experiments

Cell Viability Assay

The primary human umbilical vein endothelial cells (HUVECs) were obtained from CHI SCIENTIFIC Inc, human corneal epithelial cells (HCE-2) were purchased from the American Type culture Collection (ATCC, USA). The cell lines were cultured in a humidified incubator at 37°C under 5% CO_2 using 10 cm^2 polystyrene cell culture flasks. HUVECs were cultured in the Roswell Park Memorial Institute (RPMI) 1640 medium supplemented with 10% fetal bovine serum (FBS; Gibco, Waltham, MA, USA), 1% penicillin/streptomycin (P/S), and 2 mM L-glutamine. HCE-2 cells were cultivated in DMEM/F-12 + GlutaMAX (Gibco) supplemented with 10% FBS, epithelial growth factor (Sigma) and insulin (Sigma). The effects of ***Comp.1, Comp.2***, and NFs of ***Comp.3*** on HUVECs and HCE-2 cell viability were detected using the CCK-8 kit. Cells were seeded in a 96-well plate at a density of 1×10^4 cells/well and cultured overnight. After that, different concentrations of peptides were added into each well for another 24 h culture. Next, 10 μL of CCK-8 solution was added to each well, and the cells were incubated for another 2–4 h. The absorbance values of the solution were measured at 450 nm using a microplate reader (Multiscan FC, Thermo Fisher Scientific, Waltham, MA, USA).

Cell Proliferation Assay

HUVECs were seeded in a 96-well plate at a density of 2×10^3 cells/well. Subsequently, cells were incubated with VEGF-A (30 ng/mL) and VEGF-C (100 ng/mL) in the presence or absence of 200 μM peptides for 24 h at 37°C, and 10 μL of CCK-8 solution was added into each well. Cell proliferation was calculated using GraphPad Prism software (Version 5.0, GraphPad Software Inc., La Jolla, CA, USA) taking the untreated cells as the maximum.

Cell Tube Formation Assay

In brief, 50 μL of Matrigel (Corning, BD Biosciences, San Jose, CA, USA) was spread in a 96-well plate under cold environment and the plate was incubated at 37°C for 2 h. Cells (2.5×10^4 cells/well) were cultured in RPMI 1640 medium (Solarbio, Beijing, China) containing VEGF-A (30 ng/mL) or VEGF-C (100 ng/mL), in the presence of peptides (200 μM). An inverted (bright-field) microscope (Nikon, Tokyo, Japan) was used to evaluate the endothelial network formation per field (objective, 4×).

Animals Experiments

Establishment and Medication of Alkali-Induced CNV

The CNV model was established in mice using the alkali burn–induced injury method.[44,45] All operations and experiments were performed under general anesthesia by intraperitoneal injection of 1% pentobarbital sodium (80 mg/kg) and topical administration of 0.4% oxybuprocaine hydrochloride eye drops. The right eye's cornea was induced by placing sterilized filter paper (2 mm in diameter) soaked with 2 μL of NaOH solution (1 M) for 20 s to establish CNV model. Then, the conjunctival fornices and ocular surface were extensively flushed with 20 mL of saline. CNV was assessed one day after alkali burn injury under the slit lamp microscope (SLM-8E, Chongqing Kanghua, Chongqing, China). Subsequently, the CNV model mice were randomly divided into five groups (15 subjects per group), and their eyes were treated with 5 μL of saline, 0.25% ***Comp.1***, 0.25% ***Comp.2***, 0.5% ***gel of 3***, or Dex eye drops. All groups were treated four times a day for 7 days.

On day 7, three mice from each group were used for vessel density evaluation,[46] mice were sacrificed and their eyes were fixed with 4% paraformaldehyde, embedded in paraffin, and then sliced into sections (5 μm), which were stained with hematoxylin–eosin (H&E) dye for the purpose of observing the structure and morphology of the ocular tissue using a fluorescence microscope (Nikon 80i, Japan).

Enzyme-Linked Immunosorbent Assay (ELISA)

After 7 days alkali burn injury, corneal tissues were collected and each group consisted of five mice. Corneal tissue samples were weighed and immediately frozen at 80°C until analysis. For preparation of corneal tissue homogenate, corneal tissue samples were removed from the freezer and rewarmed at 4°C for 0.5 h. Subsequently, ophthalmic tissue scissors were utilized to cut the corneal tissue into small pieces, which were soaked in 100 μL of RIPA (Solarbio),

chilled in an ice bath for 1.5 h, and centrifuged at 12,000 rpm at 4°C for 5 min. The supernatant was transferred to another centrifuge tube for a later experiment. The protein content of VEGF-A and VEGF-C in the corneal tissue were determined using a bicinchoninic acid (BCA) kit (Solarbio), following the manufacturer's instructions. Absorbance was measured at 450 nm using a microplate reader (Multiscan FC, Thermo Fisher Scientific, Waltham, MA, USA).

Ocular Irritation and Biocompatibility

The biosafety of ***gel of 3*** in vivo were evaluated using the Draize eye test.[47] Briefly, a volume of 100 μL ***gel of 3*** was instilled into the conjunctival sac in the left eye one time, and the right eye were treated with PBS as the control. The eyes (including the redness of conjunctiva, swelling, congestion and discharge) were examined using a slit lamp (SLM-8E, Chongqing Kanghua, Chongqing, China) before each administration and 1, 2, 4, 24, 48 and 72 h after the instillation. Meanwhile, the integrity of corneal epithelium was checked using the fluorescein sodium staining assay. After the experiment, the animals were sacrificed, and the whole eyeballs were collected, and fixed in FBS Eyeball fixation solution (Servicebio, Wuhan, China) for 72 h. Then, the corneas were harvested, embedded in paraffin and cut into sections (5 μm). Finally, the sections were stained with H&E for pathological observation using a fluorescence microscope (Nikon 80i, Japan).

Statistical Analysis

All the results are expressed as the mean ± standard deviation. Groups were compared using two-way analysis of variance (ANOVA) with GraphPad Prism 5 software (Version 5.0, GraphPad Software Inc). Differences were significant at a p-value < 0.05.

Results and Discussion

Peptide Synthesis and Characterization of Self-Assembly

In the previous reported, the PCAIWF have the bioactive function of antiangiogenic, due to low solubility, we hypothesis used amphiphile peptide conjugated with PCAIWF to increase its solubility or bioactivity. Meanwhile, π–π interactions are crucial to the formation of self-assembled, short peptide–based nanomaterials and hydrogels. Short peptides based on F, FF, and FFY motifs have been widely employed to construct the nanostructure of supramolecular nanomaterials, and the amides Glu (E) and Asp (D) have been utilized to improve solubility. Herein, the PCAIWF (***Comp.1***) peptide segment was conjugated to the amphiphilic Nap-FFEE (***Comp.2***) sequence to design an effective, antiangiogenic, self-assembled peptide, Nap-FFEEPCAIWF (***Comp.3***), which could self-assemble as NFs into a hydrogel (***gel of 3***) (Scheme 1). It was hoped that ***Comp.3*** could improve the ligand-binding affinity of the bioactive peptide sequence to VEGF receptors, thereby enhancing the peptide's antiangiogenic efficacy. The chemical structures of the peptides are presented in Figure 1. The peptides were synthesized via standard Fmoc-based SPPS, and the pure peptide products were characterized and confirmed by electrospray ionization HR-MS (Supporting Information, Figures S1–S3).

According to rheological measurements in the frequency range of 0.1–100 rad s^{-1} (Figure 2A), 0.5 wt% ***gel of 3*** in phosphate-buffered saline (PBS) exhibited a storage modulus (G′) greater than its loss modulus (G″), which indicated that ***gel of 3*** possessed mechanical properties. TEM was employed to characterize the micromorphology of ***gel of 3***, revealing elongated and uniform NFs (Figure 2B) with a diameter of approximately 11 nm. CD spectroscopy was utilized to study the secondary structures of the peptides, revealing that ***gel of 3*** possessed β-sheet-like structures with peaks in the CD spectrum at approximately (+198 nm, −218 nm) (Figure 2D). However, ***Comp.2*** displayed random coil–structures with peaks in the CD spectrum that were not attributable to any classical secondary structures. These results demonstrated that the amphiphilic peptide could enhance the self-assembly ability of the hydrophobic bioactive peptide and facilitate the formation of a 3D network with NFs, which ultimately improved the peptide's solubility. The UV–Vis spectra of the peptides provided further information about the molecular arrangement of the NFs. As shown in Figure 2C, the spectra of ***Comp.2*** and ***Comp.3*** exhibited emission peaks at approximately 208 and 220 nm, while that of ***Comp.1*** showed a single emission peak at approximately 210 nm, indicating that ***Comp.2*** was conjugated with ***Comp.1***, and the obtained ***Comp.3*** could self-assemble into a nanostructure.

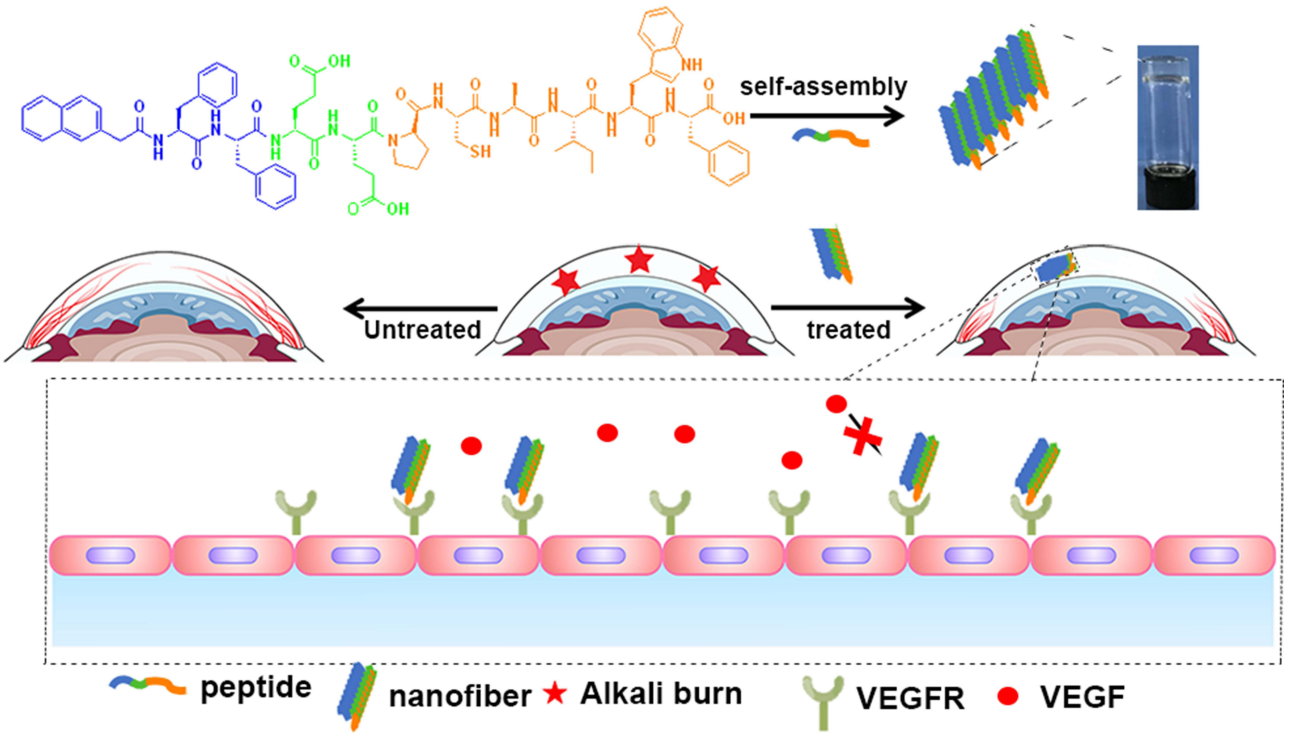

Scheme 1 Illustration of the self-assembled molecular hydrogel and nanofibers inhibiting neovascularization in a CNV model.

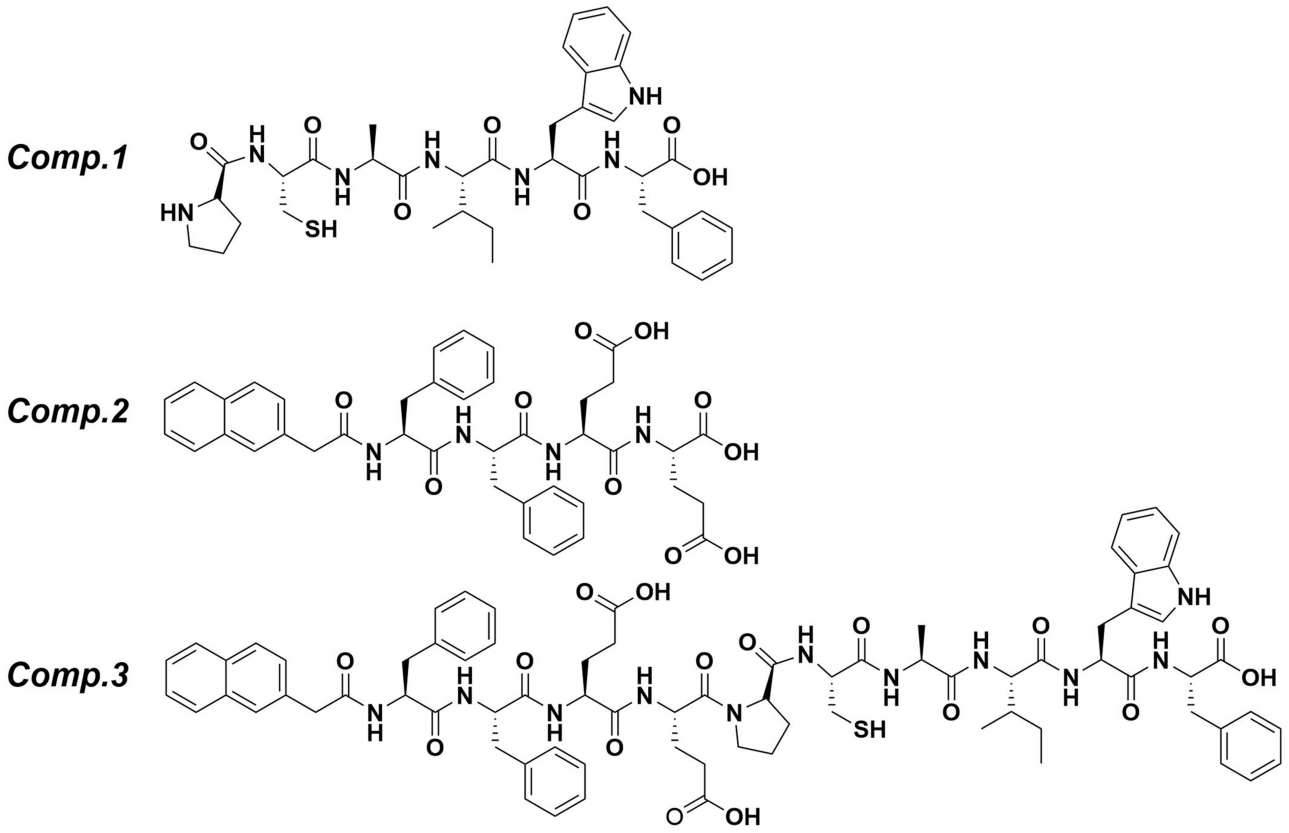

Figure 1 Chemical structures of peptides.

Cell Related Study

The viability of HCE-2 cells and HUVECs incubated with the peptides and ***gel of 3*** was determined via the CCK-8 assay. Even at concentrations >400 μM, ***Comp.1*** did not induce an obvious cytotoxic effect in cells after incubation for 24 h. After incubation with ***Comp.2*** and ***gel of 3***, the viability of HUVECs and HCE-2 cells was >80% at 200 μM (Figures 2E and S4). Subsequently, we selected a safe concentration to study the efficacy of the peptides in vitro. Angiogenesis is a complex physiological process, involving cell tube formation and mitosis. During blood vessel formation, VEGF is a potent angiogenic factor that binds to VEGFR on endothelial cells to stimulate their proliferation. As shown in Figure 2F, 200 μM NFs in the hydrogel inhibited HUVEC proliferation in the presence of VEGF-A (30 ng/mL) and VEGF-C (100 ng/mL) after incubation for 24 h. In spite of ***Comp.2*** possessing a similar ability to suppress HUVEC proliferation as ***gel of 3***, the effect may have been due to its cell toxicity. The study findings demonstrated that the amphiphilic peptide sequence was incorporated into the bioactive peptide, which formed a nanofibrous material that could interfere with endothelial cell growth, and 200 μM peptide could inhibit the HUVECs proliferation rate.

Since endothelial cells form capillary-like networks that are crucial to tissue engineering, the effect of the peptides and ***gel of 3*** on angiogenic activity was evaluated via two VEGF-induced angiogenesis assays. Because of its ease of use and ability to provide a rapid and quantitative angiogenesis estimation, Matrigel was utilized in the tube formation assay

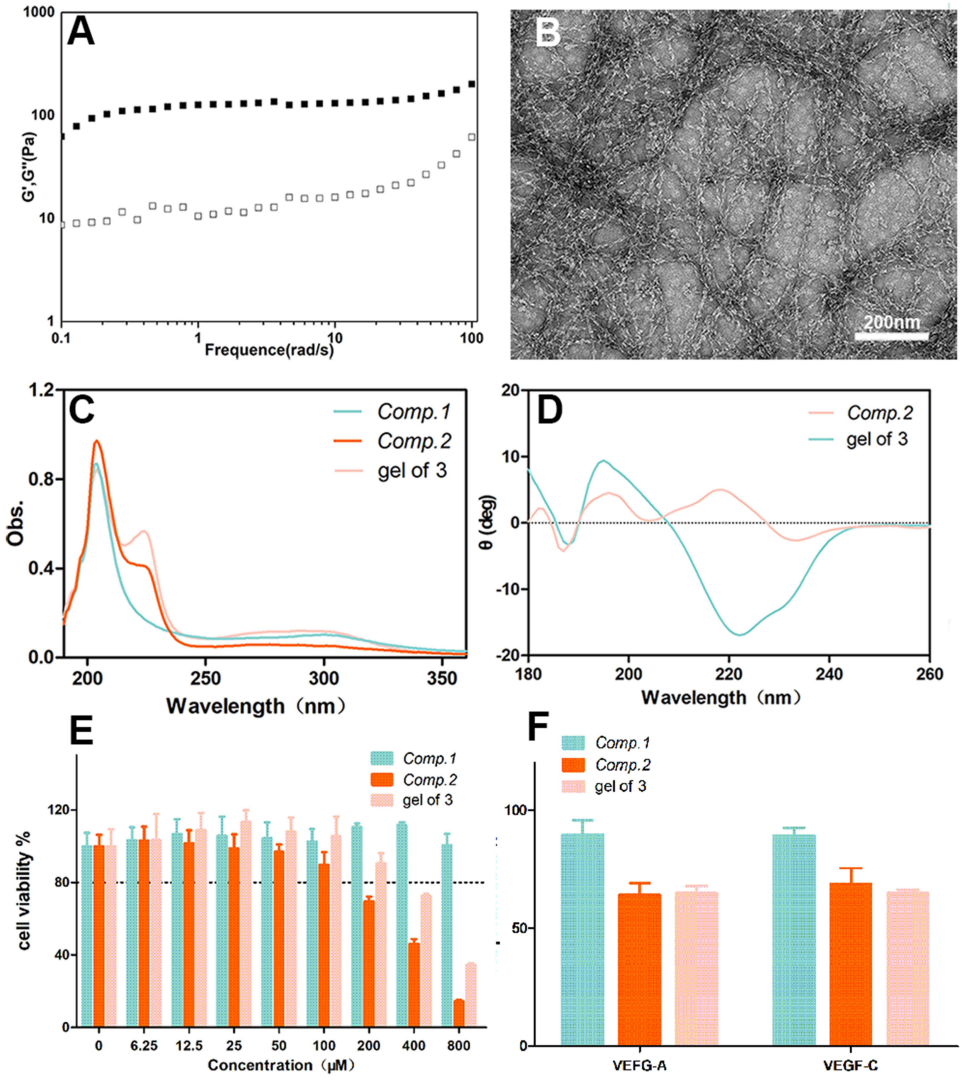

Figure 2 (**A**) Frequency sweeps of ***gel of 3***, (**B**) image of ***gel of 3*** prepared by a heating–cooling process (5 mg/mL), (**C**) UV–Vis spectra of different peptides, (**D**) Circular dichroism (CD) spectroscopy of a solution of **Comp.2** and ***gel of 3***. (**E**) In vitro cytotoxicity of peptides against HCE-2 cells after incubation for 24 h. (**F**) Proliferation rate of HUVECs inhibited by 200 μM peptides after incubation for 24 h.

as a membrane-based matrix. As shown in Figure 3, peptides with VEGF-A or VEGF-C were added on the Matrigel layer surface, then the tube formation images were taken by microscope, the tubular structure of HUVECs was reduced after incubation for 4 h with 200 μM ***Comp.1*** and ***gel of 3***, demonstrating that ***gel of 3*** efficiently inhibited VEGF-induced angiogenesis. However, ***Comp.2***, without the bioactive peptide group, did not inhibit angiogenesis. These results indicated that the self-assembled bioactive peptide could enhance the inhibition of VEGF-induced angiogenesis in vitro.

Treatment of Alkali-Induced CNV and Biocompatibility

The inhibitory effect of the peptides and ***gel of 3*** on CNV was investigated in the alkali burn–induced CNV mouse model. The burn areas and corneal defects on day 0 in images after fluorescein sodium dosing (Figure S5) were consistent across all groups, indicating that CNV modeling was successful. New vessels appearing from the corneal limbus were examined by slit lamp on days 1, 3, and 7 (Figure 4A). The CNV model established by corneal alkali burn generates corneal epithelial defects, angiogenesis, and intense inflammation in the cornea, and it has been widely used to investigate the mechanism and treatment of CNV. As shown in Figure 4A and B, new blood vessels were most pronounced at day 1 in all groups, demonstrating invasion of the central cornea and edematous tissue. A significantly reduced area of neovascularization was observed on day 7 in the ***gel of 3*** group, which was similar to that in the Dex group, with thin neovessels spanning the corneal limbus. The data presented in Figure 4C demonstrated that the neovascularization area percentage in the saline and ***Comp.2*** groups was significantly higher than that in the other treatment groups. Similarly, mice treated with ***Comp.1*** did not exhibit obviously inhibited neovascularization, similar to the ***Comp.2*** group. We hypothesized that water-insoluble ***Comp.1*** could not be sufficiently dispersed in tears and was quickly cleared, and ***Comp.2*** was not retained in the target group, which was consistent with the in vitro tube formation results. The study findings suggested that amphiphilic ***Comp.3***, created by ***Comp.2*** in conjunction with ***Comp.1***, better penetrated the superficial layers of the cornea to effectively enhance the suppression of CNV.

H&E staining was employed to investigate histological changes in the cornea, illustrating the structure of the corneal layers and any signs of abnormality. As shown in Figure 5A, Normal corneas epithelial cells were neatly arranged with regular collagen fiber arrangement in the stroma and no vascular structure or pathological changes. By contrast, inflammatory molecule infiltration and formation of new blood vessels were significantly increased in the PBS group. Corneas in the ***gel of 3*** group exhibited similar formation of new blood vessels as in the Dex group. Meanwhile, the abundance of neovessels in the ***gel of 3*** group was lower than that in the ***Comp.1*** and ***Comp.2*** groups, and the collagen fibers were changed in the ***Comp.1*** group. Nevertheless, inflammatory cells were identified in the stroma of the ***Comp.1*** group, likely because ***Comp.1*** did not exert an anti-inflammatory effect. These results indicated that, compared with

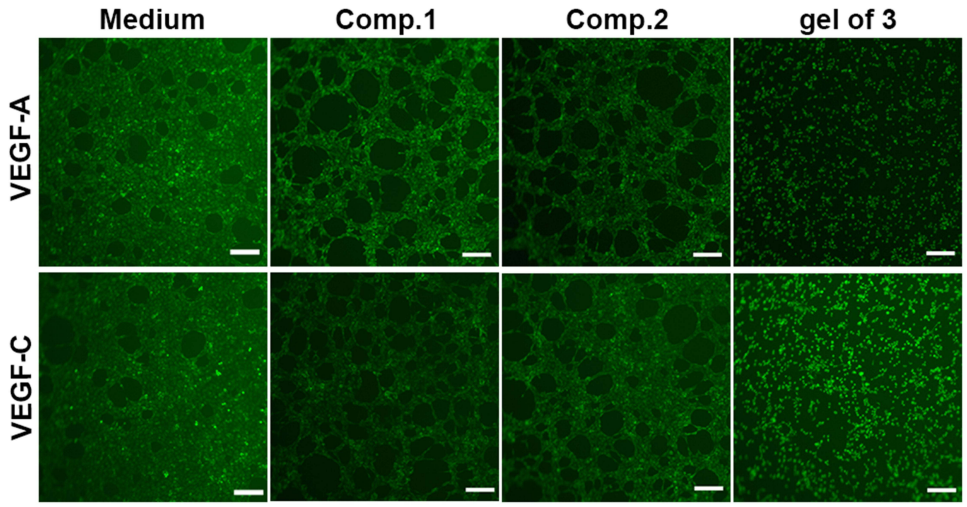

Figure 3 Matrigel tube formation of HUVECs treated with PBS (control), ***Comp.1, Comp.2***, and ***gel of 3*** at 200 μM in the presence or absence of VEGF-A (30 ng/mL) and VEGF-C(100 ng/mL). Scalebar: 200 μm.

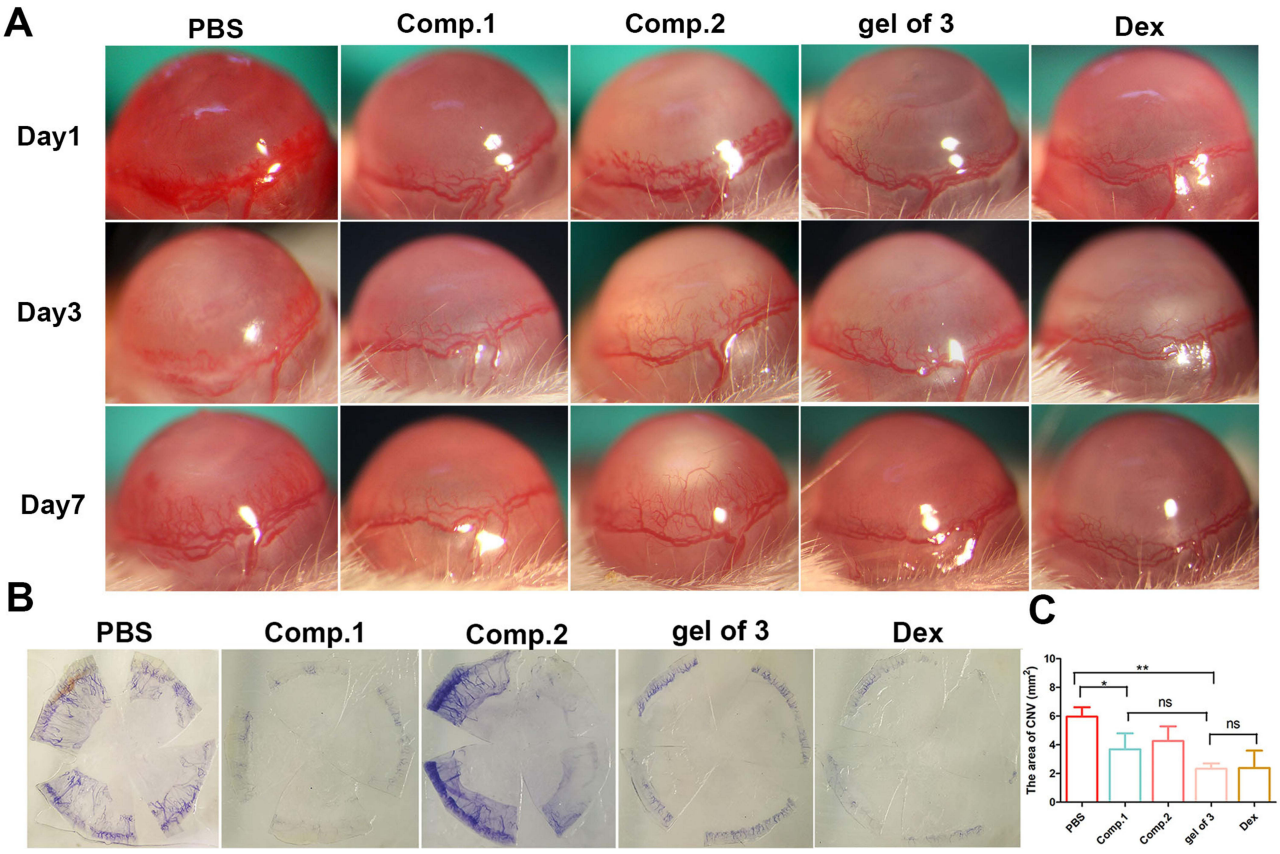

Figure 4 (**A**) Photographs of the anterior ocular segment representing morphological differences induced by different treatments; (**B**) CNV area at 7 days after alkali burn by hematoxylin perfusion; (**C**) area of corneal neovascularization at 7 days after alkali burn. Data represent the mean ± SD of three mice per group, one-way ANOVA, *$p < 0.05$, **$p < 0.01$.

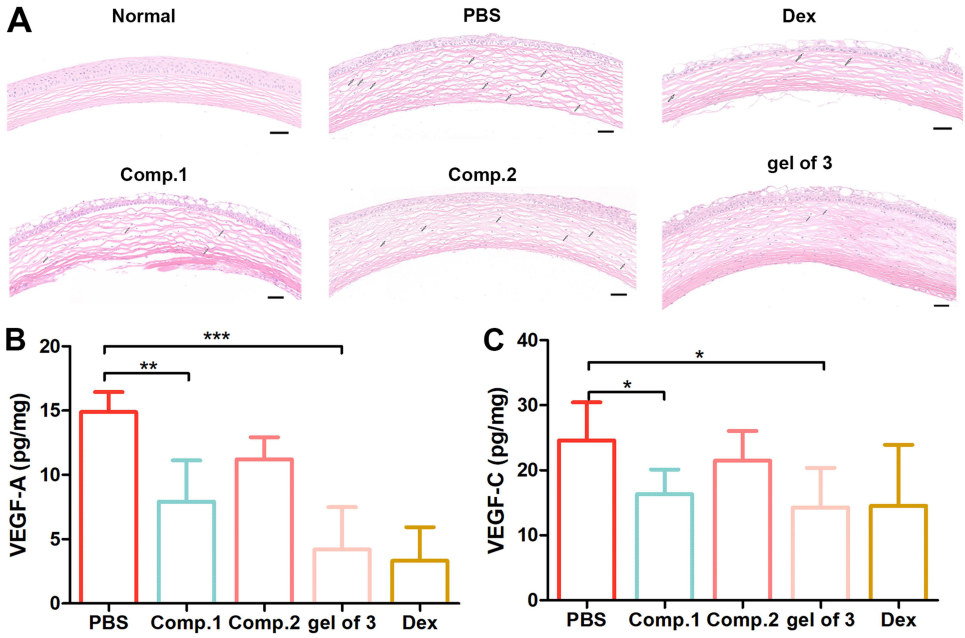

Figure 5 (**A**) Hematoxylin and eosin (H&E) staining of corneal sections in different groups, Scalebar: 50 μm; Levels of (**B**) VEGF-A and (**C**) VEGF-C determined by ELISA in corneal tissues at 7 days after alkaline-induced corneal burn. Data represent the mean ± SD of five mice per group, one-way ANOVA, *$p < 0.05$, **$p < 0.01$, ***$p< 0.001$.

insoluble ***Comp.1***, self-assembly of the amphiphilic peptide into a hydrogel provided an effective platform that could alleviate neovascularization to an extent equivalent to that of Dex by delivering bioactive peptide into the corneal tissue. Furthermore, we measured VEGF-A and VEGF-C protein levels in the cornea after 7 days via ELISA to investigate the effect of the peptides and ***gel of 3*** on protein expression in CNV model mice. As shown in Figure 5B and C, the ***gel of 3*** group exhibited lower VEGF-A ($p < 0.001$ vs saline) and VEGF-C ($p < 0.05$ vs saline) levels than the PBS group. Additionally, VEGF-A and VEGF-C levels in the ***gel of 3*** group were lower than those in the saline and ***Comp.2*** groups and similar to those in the ***Comp.1*** and Dex groups. These results suggested that the potential framework of the NFs in the hydrogel blocked VEGF-A and VEGF-C receptors, thereby exerting a substantial inhibitory effect on CNV.

As a novel peptide-based nanomaterials, it was very important to assess ocular irritation and biocompatibility before in vivo application. We carried out to examined the ocular irritation to further evaluate the biosafety of ***gel of 3***. As shown in Figure S6, there were not exist redness, inflammation or swelling in the eye signs of ocular irritation in the eye, which indicating the non-irritation of ***gel of 3***, and the fluorescein staining exhibited no sign of damage was observed to the cornea or conjunctivae. Moreover, the histological examination provided further evidence that the treatment of the ***gel of 3*** preserved the completed corneal structure and no abnormality of tissues in the corneal, conjunctiva and iris compared with PBS group at 72 h. All these finding suggested that NFs of ***gel of 3*** did not irritation or toxicity to eye.

Conclusion

In this study, we describe the development of a novel amphiphilic peptide based on the new-found bioactive ***Comp.1*** peptide, which self-assembled into a supramolecular hydrogel with orderly arranged NFs. The self-assembled NFs demonstrated enhanced antiangiogenic bioactivity compared to free insoluble ***Comp.1*** in vitro and in vivo, possibly because of the ordered organization of the bioactive sequences in peptide NFs. In addition, the self-assembled NFs may increase the half-life period of developed drugs by slowing down the enzymatic degradation of bioactive peptides. Moreover, the NFs exerted no obvious toxicity in corneal epithelial cells, and showed good ocular tolerance and biocompatibility in eye. Taken together, the study findings indicate that the NFs of ***gel of 3*** provide an effective approach for improving the therapeutic efficacy of free peptide–based drugs against CNV, which may potentially be utilized for the treatment of ocular vascular diseases and other angiogenesis-related diseases.

Acknowledgments

This work is supported by the Henan Provincial Medical Science and Technology Program (LHGJ20200063), the Henan Eye Hospital Basic Science Research Program (22JCQN008), and the Henan Provincial Key Project of Medical Science and Technology Program (SBGJ202102050).

Disclosure

The authors declare that there are no conflicts of interest in this work.

References

1. Ambati BK, Nozaki M, Singh N, et al. Corneal avascularity is due to soluble VEGF receptor-1. *Nature*. 2006;443(7114):993–997. doi:10.1038/nature05249
2. Ouyang H, Xue Y, Lin Y, et al. WNT7A and PAX6 define corneal epithelium homeostasis and pathogenesis. *Nature*. 2014;511(7509):358–361. doi:10.1038/nature13465
3. Imanishi J, Kamiyama K, Iguchi I, Kita M, Sotozono C, Kinoshita S. Growth factors: importance in wound healing and maintenance of transparency of the cornea. *Prog Retinal Eye Res*. 2000;19(1):113–129. doi:10.1016/S1350-9462(99)00007-5
4. Chang JH, Garg NK, Lunde E, Han KY, Jain S, Azar DT. Corneal neovascularization: an anti-VEGF therapy review. *Surv Ophthalmol*. 2012;57(5):415–429. doi:10.1016/j.survophthal.2012.01.007
5. Abdelfattah NS, Amgad M, Zayed AA, et al. Clinical correlates of common corneal neovascular diseases: a literature review. *Int J Ophthalmol*. 2015;8(1):182–193. doi:10.3980/j.issn.2222-3959.2015.01.32
6. Ellenberg D, Azar DT, Hallak JA, et al. Novel aspects of corneal angiogenic and lymphangiogenic privilege. *Prog Retinal Eye Res*. 2010;29(3):208–248. doi:10.1016/j.preteyeres.2010.01.002
7. Liu CH, Wang Z, Sun Y, Chen J. Animal models of ocular angiogenesis: from development to pathologies. *FASEB J*. 2017;31(11):4665–4681. doi:10.1096/fj.201700336R
8. Skobe M, Dana R. Blocking the path of lymphatic vessels. *Nat Med*. 2009;15(9):993–994. doi:10.1038/nm0909-993

9. Bock F, Matthaei M, Reinhard T, et al. High-dose subconjunctival cyclosporine a implants do not affect corneal neovascularization after high-risk keratoplasty. *Ophthalmology*. 2014;121(9):1677–1682. doi:10.1016/j.ophtha.2014.03.016
10. West XZ, Malinin NL, Merkulova AA, et al. Oxidative stress induces angiogenesis by activating TLR2 with novel endogenous ligands. *Nature*. 2010;467(7318):972–976. doi:10.1038/nature09421
11. Oh J, Takahashi R, Kondo S, et al. The membrane-anchored MMP inhibitor RECK is a key regulator of extracellular matrix integrity and angiogenesis. *Cell*. 2001;107(6):789–800. doi:10.1016/S0092-8674(01)00597-9
12. Maybee DV, Ink NL, Ali MAM. Novel roles of mt1-mmp and mmp-2: beyond the extracellular milieu. *int j mol sci*. 2022;23(17):9513. doi:10.3390/ijms23179513
13. Shalaby F, Rossant J, Yamaguchi TP, et al. Failure of blood-island formation and vasculogenesis in flk-1-deficient mice. *Nature*. 1995;376 (6535):62–66. doi:10.1038/376062a0
14. Li X, Sun X, Carmeliet P. Hallmarks of endothelial cell metabolism in health and disease. *Cell Metab*. 2019;30(3):414–433. doi:10.1016/j.cmet.2019.08.011
15. Ricci F, Bandello F, Navarra P, Staurenghi G, Stumpp M, Zarbin M. Neovascular age-related macular degeneration: therapeutic management and new-upcoming approaches. *Int J Mol Sci*. 2020;21(21):8242. doi:10.3390/ijms21218242
16. Ahmad A, Nawaz MI. Molecular mechanism of VEGF and its role in pathological angiogenesis. *J Cell Biochem*. 2022;123(12):1938–1965. doi:10.1002/jcb.30344
17. Zhou W, Liu K, Zeng L, et al. Targeting VEGF-A/VEGFR2 Y949 signaling-mediated vascular permeability alleviates hypoxic pulmonary hypertension. *Circulation*. 2022;146(24):1855–1881. doi:10.1161/CIRCULATIONAHA.122.061900
18. Huang D, Liu G, Xu Z, et al. The multifaceted role of placental growth factor in the pathogenesis and progression of bronchial asthma and pulmonary fibrosis: therapeutic implications. *Genes Dis*. 2023;10(4):1537–1551. doi:10.1016/j.gendis.2022.10.017
19. Siktberg J, Kim SJ, Sternberg P Jr, Patel S. Effectiveness of bevacizumab step therapy for neovascular age-related macular degeneration. *Eye*. 2023;37(9):1844–1849. doi:10.1038/s41433-022-02253-6
20. Craik DJ, Fairlie DP, Liras S, Price D. The future of peptide-based drugs. *Chem Biol Drug Des*. 2013;81(1):136–147. doi:10.1111/cbdd.12055
21. Budzinskaya MV, Plyukhova AA, Sorokin PA. Anti-VEGF therapy resistance in neovascular age-related macular degeneration. *Vestnik oftalmologii*. 2017;133(4):103–108. doi:10.17116/oftalma20171334103-108
22. ElSheikh RH, Chauhan MZ, Sallam AB. Current and novel therapeutic approaches for treatment of neovascular age-related macular degeneration. *Biomolecules*. 2022;12(11):1629. doi:10.3390/biom12111629
23. Freund KB, Mrejen S, Gallego-Pinazo R. An update on the pharmacotherapy of neovascular age-related macular degeneration. *Expert Opin Pharmacother*. 2013;14(8):1017–1028. doi:10.1517/14656566.2013.787410
24. Kuai R, Li D, Chen YE, Moon JJ, Schwendeman A. High-density lipoproteins: nature's multifunctional nanoparticles. *ACS nano*. 2016;10 (3):3015–3041. doi:10.1021/acsnano.5b07522
25. Fosgerau K, Hoffmann T. Peptide therapeutics: current status and future directions. *Drug Discov Today*. 2015;20(1):122–128. doi:10.1016/j.drudis.2014.10.003
26. Gattringer J, Gruber CW, Hellinger R. Peptide modulators of cell migration: overview, applications and future development. *Drug Discov Today*. 2023;28(5):103554. doi:10.1016/j.drudis.2023.103554
27. Zhang K, Zhang H, Gao YH, et al. A monotargeting peptidic network antibody inhibits more receptors for anti-angiogenesis. *ACS nano*. 2021;15 (8):13065–13076. doi:10.1021/acsnano.1c02194
28. Hu Y, Shi H, Ma X, et al. Highly stable fibronectin-mimetic-peptide-based supramolecular hydrogel to accelerate corneal wound healing. *Acta Biomater*. 2023;159:128–139. doi:10.1016/j.actbio.2023.01.047
29. Chen Z, Mao X, Ye X, et al. A novel and biocompatible nanofiber of VEGF peptide for enhanced corneal neovascularization suppression. *Chem Eng J*. 2021;416:129081. doi:10.1016/j.cej.2021.129081
30. Silva RLE, Kanan Y, Mirando AC, et al. Tyrosine kinase blocking collagen IV-derived peptide suppresses ocular neovascularization and vascular leakage. *Sci Trans Med*. 2017;9:eaai8030 doi:10.1126/scitranslmed.aai8030.
31. Dong A, Seidel C, Snell D, et al. Antagonism of PDGF-BB suppresses subretinal neovascularization and enhances the effects of blocking VEGF-A. *Angiogenesis*. 2014;17(3):553–562. doi:10.1007/s10456-013-9402-5
32. Michaloski JS, Redondo AR, Magalhães LS, Cambui CC, Giordano RJ. Discovery of pan-VEGF inhibitory peptides directed to the extracellular ligand-binding domains of the VEGF receptors. *Sci Adv*. 2016;2(10):e1600611. doi:10.1126/sciadv.1600611
33. Karavasili C, Fatouros DG. Self-assembling peptides as vectors for local drug delivery and tissue engineering applications. *Adv Drug Delivery Rev*. 2021;174:387–405. doi:10.1016/j.addr.2021.04.024
34. Zhang Z, Ai S, Yang Z, Li X. Peptide-based supramolecular hydrogels for local drug delivery. *Adv Drug Delivery Rev*. 2021;174:482–503. doi:10.1016/j.addr.2021.05.010
35. Gao J, Zhan J, Yang Z. Enzyme-instructed self-assembly (eisa) and hydrogelation of peptides. *Adv Mater*. 2020;32(3):e1805798. doi:10.1002/adma.201805798
36. Wang Y, Cheetham AG, Angacian G, Su H, Xie L, Cui H. Peptide-drug conjugates as effective prodrug strategies for targeted delivery. *Adv Drug Delivery Rev*. 2017;110–111:112–126. doi:10.1016/j.addr.2016.06.015
37. Shigemitsu H, Hamachi I. Design strategies of stimuli-responsive supramolecular hydrogels relying on structural analyses and cell-mimicking approaches. *Acc Chem Res*. 2017;50(4):740–750. doi:10.1021/acs.accounts.7b00070
38. Qiu R, Sasselli IR, Álvarez Z, et al. Supramolecular copolymers of peptides and lipidated peptides and their therapeutic potential. *J Am Chem Soc*. 2022;144(12):5562–5574. doi:10.1021/jacs.2c00433
39. Raskatov JA, Schneider JP, Nilsson BL. Defining the landscape of the Pauling-Corey rippled sheet: an orphaned motif finding new homes. *Acc Chem Res*. 2021;54(10):2488–2501. doi:10.1021/acs.accounts.1c00084
40. Bera S, Gazit E. Self-assembly of functional nanostructures by short helical peptide building blocks. *Protein Pept Lett*. 2019;26(2):88–97. doi:10.2174/0929866525666180917163142
41. Ding Y, Zheng D, Xie L, et al. Enzyme-instructed peptide assembly favored by preorganization for cancer cell membrane engineering. *J Am Chem Soc*. 2023;145(8):4366–4371. doi:10.1021/jacs.2c11823

42. Zhang J, Gao J, Chen M, Yang Z. Using phosphatases to generate self-assembled nanostructures and their applications. *Antioxid Redox Signaling*. 2014;20(14):2179–2190. doi:10.1089/ars.2013.5701
43. Wang Z, Wang Q, Cao H, et al. Mitochondrial localized in situ self-assembly reprogramming tumor immune and Metabolic microenvironment for enhanced cancer therapy. *Adv Mater*. 2024;36(15):2311043. doi:10.1002/adma.202311043
44. Giacomini C, Ferrari G, Bignami F, Rama P. Alkali burn versus suture-induced corneal neovascularization in C57BL/6 mice: an overview of two common animal models of corneal neovascularization. *Exp Eye Res*. 2014;121():1–4. doi:10.1016/j.exer.2014.02.005
45. Tian S, Wang S, He Y, et al. Review of the progress in corneal neovascularization animal models. *Am J Biochem Biotechnol*. 2015;11(4):221–227. doi:10.3844/ajbbsp.2015.221.227
46. Luo Q, Yang J, Xu H, Shi J, Liang Z, Zhang R, Lu P, Pu G, Zhao N, Zhang J. (2022). Sorafenib-loaded nanostructured lipid carriers for topical ocular therapy of corneal neovascularization: development, in-vitro and in vivo study. Drug Delivery, 29(1), 837–855. 10.1080/10717544.2022.2048134
47. Alasino RV, Garcia LG, Gramajo AL, Pusterla JP, Beltramo DM, Luna JD. Ocular biocompatibility of polyquaternium 10 gel: functional and morphological results. *J Mater Sci Mater Med*. 2015;26(2):64. doi:10.1007/s10856-014-5358-2